

EgoReID Dataset: Person Re-identification in Videos Acquired by Mobile Devices with First-Person Point-of-View

Emrah Basaran^{1*}

Yonatan Tariku Tesfaye^{2*}

Mubarak Shah²

basaranemrah@itu.edu.tr

yonatantariku@knights.ucf.edu

shah@crcv.ucf.edu

¹Dept. of Computer Engineering, Istanbul Technical University

²Center for Research in Computer Vision, University of Central Florida

Abstract

In recent years, we have seen the performance of video-based person Re-Identification (ReID) methods have improved considerably. However, most of the work in this area has dealt with videos acquired by fixed cameras with wider field of view. Recently, widespread use of wearable cameras and recording devices such as cellphones have opened the door to interesting research in first-person Point-of-view (POV) videos (egocentric videos). Nonetheless, analysis of such videos is challenging due to factors such as poor video quality due to ego-motion, blurriness, severe changes in lighting conditions and perspective distortions. To facilitate the research towards conquering these challenges, this paper contributes a new dataset called EgoReID. The dataset is captured using 3 mobile cellphones with non-overlapping field-of-view. It contains 900 IDs and around 10,200 tracks with a total of 176,000 detections. The dataset also contains 12-sensor meta data e.g. camera orientation pitch and rotation for each video.

In addition, we propose a new framework which takes advantage of both visual and sensor meta data to successfully perform Person ReID. We extend image-based re-ID method employing human body parsing trained on ten datasets to video-based re-ID. In our method, first frame level local features are extracted for each semantic region, then 3D convolutions are applied to encode the temporal information in each sequence of semantic regions. Additionally, we employ sensor meta data to predict targets' next camera and their estimated time of arrival, which considerably improves our ReID performance as it significantly reduces our search space.



Figure 1: (a) shows three tracklets of the same identity from the same camera, its evident to see that due to both camera and target motions the target is captured in different poses, backgrounds and illuminations. (b) each row shows tracklets of the same identity captured from camera 1, 2 and 3, respectively. Due to close proximity of target and the cameras, different body regions of the target are missing in Camera 1 and 2.

1. Introduction

Person Re-Identification (ReID) aims at associating the same pedestrian across multiple cameras [20, 62]. This task has drawn increasing attention in recent years due to its importance in applications, such as surveillance [50], activity analysis [34] and tracking [56]. Person ReID remains a challenging problem because of complex variations in camera viewpoints, human poses, lighting, occlusions, and background clutter.

Currently, in almost all attempts to solve person ReID

* Authors contributed equally

problem, the source of data is from *fixed* cameras with wider field of view (FOV). Mostly, in such datasets, full bodies of pedestrians are captured and intra camera variations of targets are very small, as pose of targets often do not change within the same camera. On the contrary, videos from a moving first-person point-of-view (POV) devices pose unique challenges, such as frequent occlusion of targets due to close proximity of camera and targets, blurriness caused by camera motion, severe lighting and background changes, both within and across cameras, appearance differences due to different perspectives. Moreover, due to constant motion of both target and cameras, there are frequent inter camera appearance changes between sequences of the same target. This is mainly due to the fact that a target can appear in several poses in a single camera view as shown in Fig. 1 (a).

Besides the unique challenges posed by the nature of the video, these devices (such as cellphones) provide additional source of information. Most new generation devices are equipped with additional sensors such as gyros, accelerometers, magnetometers, GPS and are Internet-enabled, it is now possible to obtain large amounts of first-person point-of-view (POV) data un-intrusively.

In order to facilitate the research towards such unique video domain, In this paper, we propose a new dataset called EgoReID. Different from existing datasets EgoReID has several new features. 1) 3 synchronized mobile cellphones with non-overlapping FOV are used to record the videos. 2) Throughout the recording, all 3 cameras are moving around campus covering larger area, resulting in complex scene transformation and background. 3) 12 sensor meta data along with the videos are also collected. 4) YOLO9000 [38] and FCDSC [46] are used for pedestrian detection and tracklet generation, respectively, which will be provided with the dataset.

Besides the new dataset, we propose a novel approach to leverage network trained on 10 *image-based* ReID datasets for *video-based* Person Re-ID problem. Here, we employ a model, trained on these image-based datasets, to extract frame level local features for each semantic region, then we employ 3D convolutions to encode the temporal information in each sequence of regions. Instead of directly encoding the whole sequence, we extract features from each body regions to learn discriminative local features. We then scale each local feature with their corresponding learned weights.

In addition to traditional video features, we successfully demonstrate the use of sensor *meta data* to complement appearance cues. In particular, we use meta data information to estimate target's next camera and its time of arrival, that way we significantly reduce the search space by pruning several unreliable matches which violate the estimated time of arrival constraint.

The contributions of this paper can be summarized as

follows:

- A unique and challenging EgoReID dataset is presented and will be publicly released with detections, tracks and sensor meta data.
- We propose a new model to solve person ReID problem in egocentric videos, where per frame human semantic parsing is employed to encode local visual cues. Then we extract video feature representations by aggregating the temporal information within each sequence of body parts.
- We propose a method to employ sensor meta data information to significantly reduce our search space by first predicting the next camera where the target may appear, then estimating its time of arrival.

2. Related Works

In this section, we review related works in the areas of video-based person re-identification and egocentric vision.

Video-based person re-identification: The success of deep learning in wide range of computer vision areas has been inspiring a lot of studies in person re-identification. In recent years, researchers are considering more realistic scenarios such as larger dataset [61, 59], complex scenarios [63, 39] and combining different modalities such as text descriptions in their approaches [64, 28]. The effectiveness of Convolutional Neural Network (CNN) in learning discriminative image representations from large scale datasets have been exploited effectively in [47, 48, 33, 26, 11, 58, 66]. Utilization of video data is further facilitated by the powerful feature learning ability of Convolutional Neural Networks. In video-based ReID [37, 66, 54, 49, 67, 36], the learning algorithm is given a pair of video sequences instead of images. Authors in [37] introduce an RNN model to encode temporal information. The features from all timesteps are then combined using temporal pooling to compute an overall appearance feature for the complete sequence and then the feature similarity of two videos is computed. In [49] the most discriminative video fragments are selected from noisy/incomplete image sequences of people from which reliable space-time and appearance features are computed, whilst simultaneously learning a video ranking function for person ReID. Authors in [36], introduce a new space-time person representation by encoding multiple granularities of spatio-temporal dynamics in form of time series. In [66] attention weights are combined per-frame with visual features and the forward propagated RNN hidden variables, in order to weaken the influence of the noisy samples. Authors in [52] employ spatial pooling layer to select regions from each frame, while temporal attention pooling is performed to select informative frames in the sequence. In [43], the dual attention mechanism is used,

in which both intra-sequence and inter-sequence attention strategies are employed for feature refinement and feature-pair alignment, respectively.

Unlike most of the above approaches, our proposed method assigns weights to each local feature extracted from different body regions based on their discriminative abilities. Due to lack of large number of re-ID video datasets, we leverage image-based re-ID model trained on 10 datasets and encode temporal information in each body region by applying 3D convolutions. Moreover, we employ sensor meta-data to further improve our ReID performance.

Egocentric vision: Recently, visual analysis of egocentric videos has been a hot topic in computer vision, and the work ranging from object detection [15] to recognizing daily activities [14, 13], predicting gaze behavior [32, 8], and video summarization [35] have been proposed. In [18], depth perception and 3D reconstruction are improved by fusing information from egocentric and exocentric vision with laser range data. Moreover, the relationship between moving and static cameras have been studied in some works. Authors in [3, 2] improve object detection accuracy by exploring the relationship between mobile and static cameras. Authors in [7] localize egocentric field-of-views using first-person point-of-view devices by matching images and video with the reference corpus, and refine the results using the first-persons head orientation information, obtained using the sensor devices.

Authors in [4] propose a framework for the identification of egocentric viewers, by matching and assigning the viewers among the egocentric videos and a top view video. In [53], authors introduced a new egocentric dataset for the traffic accident detection and proposed an unsupervised framework to detect the accidents from egocentric videos. In [1], multiple face tracking problem is addressed employing the sequences of egocentric videos. Using egocentric videos captured by single camera, authors in [23] propose a method to infer 3D full body pose. Authors in [17], collected a ReID dataset using the front camera of an eye tracking device. They collected images of 8 persons with around 100 images each.

To the best of our knowledge no work has been reported on video-based person ReID in egocentric videos. This probably is due to the lack of such a dataset. Therefore, proposed work will fill in an important gap in the literature.

3. EgoReID Dataset

In this section, we introduce our new EgoReID dataset.

3.1. Dataset Description

Data collection: We recorded the videos using 3 synchronized Samsung mobile cellphones with non-overlapping field of views. Throughout the period of recording, all 3 cameras were constantly moving around and covered larger

area. The videos are recorded for ~ 20 minutes with 30 fps.

Data preparation: We first detect pedestrians from the videos using Yolo9000 person detector [38]. We manually verify the detection results by removing bounding boxes which do not contain a person. Then, we employ FCDSC [46] tracker to generate tracks. Similarly, here also we manually verify tracks generated by FCDSC using the following criteria: 1) we remove tracks which are shorter than 16 frames. 2) tracks which do not contain the target for more than 80% of the track (containing $>20\%$ false positive) are removed. 3) the detection bounding box from a track is removed if target is occluded for more than 80%. During labeling, we manually assign the same label for track of the same person in different cameras. Three people were involved during both data collection and preparation. Each person has spent around 160 hours to finalize the dataset generation.

EgoReID dataset consists of around 900 different identities with 10,200 tracklets with a total of 176,000 human detection bounding boxes. Camera 1 and 2 have 190 IDs in common while camera 2 and 3 share 256 IDs in common. Around 103 IDs are present in all three cameras. 3164, 2748 and 4353 tracklets are present in camera 1,2 and 3, respectively. Each camera has around 36,000 frames. Each pedestrian detection crops have different sizes. The largest crop is 1080×1496 (width \times height), as cameras are very close to pedestrians, they often cover most of the frame. While the smallest detection is 51×38 .

Moreover, the dataset contains 12 sensor meta data, namely, Longitude, Latitude, Speed, Distance, Time, Accelerometer, Heading, Gyro, Magnetic, Gravity, Orientation and Rotation vectors. Please refer to Fig. 2.

Table 1 summarizes the statistics of existing datasets acquired by both fixed and mobile (with First-person POV) cameras. As can be seen from the table, our dataset is the first and large Video-based egocentric dataset.

Evaluation protocol: Similar to most of previous datasets, we utilize the Cumulative Matching Characteristics (CMC) curve to evaluate the ReID performance. For each query, multiple true positives could be returned. Therefore, we also consider person ReID as a retrieval task, and also employ mean Average Precision (mAP) as the evaluation metric.

4. Proposed Method

This section briefly presents the proposed model which consists of 3 main components: frame-level feature extraction, semantic segmentation and video-level weighted feature extraction. The overview of the proposed network is shown in Figure 3.

Among existing ReID datasets which are collected using fixed camera, we only consider **video-based** ReID datasets to be included in table 1.

Datasets	Fixed Cameras			Mobile Cameras	
	MARS	iLIDS	PRID	Fergani et al. [17]	EgoReID (Ours)
Number of IDs	1,261	300	200	8	900
Tracklets #	20,478	600	400	-	10,200
Camera #	6	2	2	1	3
Generated by	DPM[16]+GMMCP [12]	hand	hand	DPM [16]	Yolo9000 [38]+FCDSC [46]
Evaluation	mAP + CMC	CMC	CMC	mAP	mAP + CMC
Mode	Video-based	Video-based	Video-based	Image-based	Video-based
Meta-data	-	-	-	-	12 sensor meta-data

Table 1: Summary of datasets acquired by both fixed and mobile cameras.

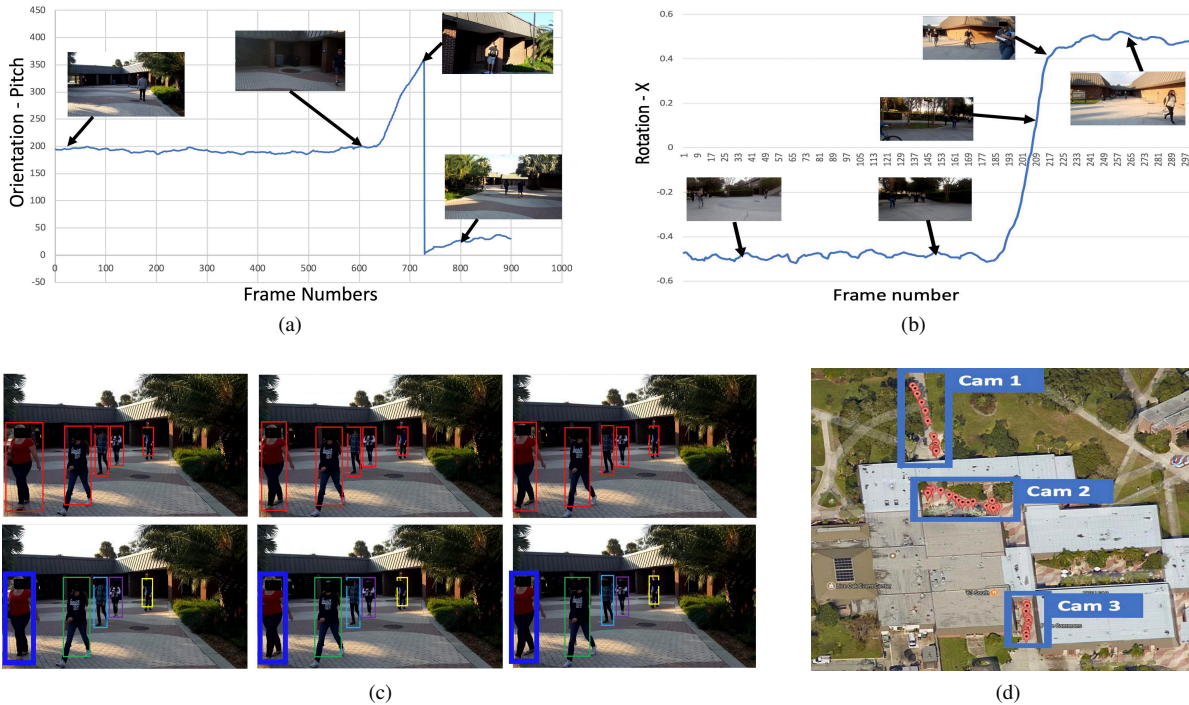


Figure 2: (a) and (b) respectively show Camera orientation-pitch Camera rotations around x axis as a functions of time (frame number). We also show corresponding images at different frames. (c) Top row shows sample human detection results and corresponding tracking results are shown in the bottom row (each track is shown by a different color). (d) shows sample GPS locations of three cameras as red dots.

Our model is inspired by the model in [24], where human parsing is successfully applied in image-based ReID. Important feature of their model is that it is trained on ten different datasets providing robust system. In the unique nature of our dataset, since targets are close to the cameras, different body regions of a target are reasonably visible, therefore above method is pretty suitable for our problem. However, their method is image-based, in this paper, we extend their method to videos and achieve significantly better results as compared to the existing state-of-the-art methods.

Since we do not have video level semantic segmentation

annotations, it is not possible to inflate [9] the bottom 2D layers to 3D, such that network accepts a video clip instead of an image and generates its single compact representation. we do not have video level semantic segmentation annotations. Therefore, we apply feature extraction and semantic segmentation at frame level first and then pool each feature map using different segmentation regions. This is followed by 3D convolution over feature activation map, with attention applied to each region, to better encode the temporal information in the video sequence. Finally, each feature vector is scaled with its corresponding learned weight.

Below, first we describe Frame-level feature Extraction and Semantic Segmentation Modules followed by video feature extraction module.

4.1. Frame-level feature extraction module:

In our model, we adopt Inception-V3 [45] as a backbone of our feature extraction module. Given a video sequence $\mathcal{X} \in \mathbb{R}^{H \times W \times 3 \times S}$ of length S , where each frame (RGB) is of size $H \times W$, which is passed to Inception-V3 to produce the frame-level feature maps. Feature maps from the Inception-V3, are then scaled up to the size of the segmentation maps, using bilinear interpolation.

4.2. Semantic segmentation module:

Similar to feature extraction module, for the segmentation module, we use the Inception-V3 architecture. However, we make two important modification to this architecture compared to the one used for feature extraction. The first modification is that the output stride of the model is reduced from 32 to 16 to get the feature maps with adequate resolution for semantic segmentation task. The extra computation cost resulting from this modification is eliminated by the replacing the convolutions in the last Inception block with the dilated convolutions [55]. The second modification is the use of atrous spatial pyramid pooling [10], instead of global average pooling to exploit multi-scale information. Unlike authors in [24], where they used 5 body regions and train their ReID model on a single classifier, in our model, we use three body regions: foreground, upper and lower body, and train a separate classifier for each body region.

4.3. Video feature extraction module:

In this module, we first extract video features by aggregating the temporal information within each sequences using a series of 3D-convolution blocks. Then, we learn weights for each region features. Fig. 4 depicts the proposed video feature extraction module.

Video features: An input to this module is three sequences of feature maps each representing different body regions. We then pass them through three separate blocks of 3D-convolutions, each with $1 \times 1 \times 3$ kernel size with spatial and temporal stride of 1 and 2, respectively. To exploit multi-scale information, we concatenate feature maps from the intermediate and final layer resulting ($30 \times 30 \times 2048$) feature map representation for each body region. We do not share weights between 3D-convolution blocks of different body region.

Feature weighting: In EgoReID, it is more often that different body regions get occluded/absent due to close proximity of camera and target. Thus, it is important that features from different regions are carefully weighted based on

their significance. For each video features, we learn their corresponding weights using shared blocks of three 2D-convolution. Finally, after applying global average pooling (GAP) on the feature maps generated by our video feature extractor, we scale them using their corresponding weights.

During training of the model, we pass the 3 feature vectors of the body regions to different soft-max layers that do not share weights and compute the classification losses separately.

5. Employing Sensor Meta-data

In this section, we discuss the proposed method for employing sensor meta data information to further help refine our re-identification results. In particular, we use the heading, speed and GPS (longitude and latitude) of the camera, which are captured by our recording devices.

Let T_a^i represents tracklet of person a in camera i . Its trajectory is given by a set of detections $T_a^i = [d_{a,t^s}^i, \dots, d_{a,t^\tau}^i]$, where d_{a,t^s}^i and d_{a,t^τ}^i represent detections of person a at time of entry and exit from camera i , respectively. $\rho(T_a^i)$ denote appearance feature representation of tracklet T_a^i generated by the proposed model. GPS and heading of camera i , \mathbb{C}^i , at time t^τ are respectively represented by $\mathbb{C}_{t^\tau}^{i^g}$ and $\mathbb{C}_{t^\tau}^{i^h}$. The heading of a target a in camera i , H_a^i , is inferred from the camera i 's heading at time t^τ , that is, if target is moving in the same direction as camera (target is walking away from the camera), then $H_a^i = \mathbb{C}_{t^\tau}^{i^h}$. Where as, if a target is moving towards the camera, like the target in Fig. 5, then $H_a^i = \mathbb{C}_{t^\tau}^{i^h} + 180^\circ$, that is, we assign the opposite heading w.r.t the camera's heading. The direction of target's movement is determined from the tracklet direction.

Estimating the next camera: Naïvely, one can select the closest camera to the target at time, t^τ , as the next camera without considering the target's direction of motion. As can be seen from the example in Figure.5, such approach will end up selecting the wrong camera k , which is located on the other side of the target. So, first, we need to select candidate cameras which are spatially located in the direction of target's heading. Then, we select the closest camera among those based on their GPS distance from the target at time t^τ . In this set up, we not only select the closest camera but also we ensure the next camera is located along the way of target's motion.

Lets define a function $\mathbb{F}(GPS_1, GPS_2)$, which returns heading angle between two GPS points. In particular, it determines which direction GPS_2 is located w.r.t GPS_1 and is computed as follows:

$$\mathbb{F}(GPS_1, GPS_2) = atan2(X, Y),$$

where,

$$X = \sin(\lambda_2 - \lambda_1) * \cos(\varphi_2),$$

$$Y = \cos(\varphi_1) * \sin(\varphi_2) - \sin(\varphi_1) * \cos(\varphi_2) * \cos(\lambda_2 - \lambda_1).$$

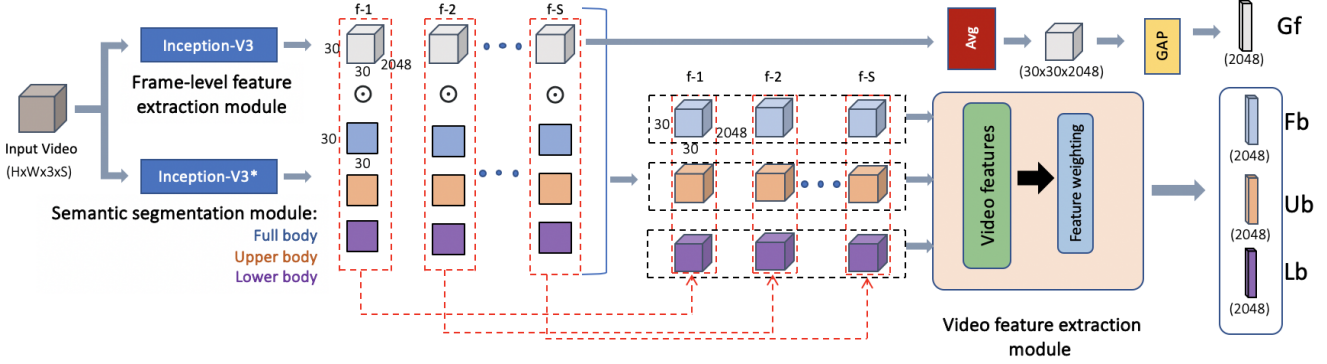


Figure 3: Proposed Network: First, the input video clip consisting of S frames is input to the Inception-V3 models, the feature maps and 3 segmentation maps for each frame (f-1 to f-S) are generated in the upper and lower branches of the model, respectively. We pool the feature maps using segmentation maps and obtain sequences of 3 feature maps, each focusing on a different body regions: lower, upper and full. Next, we encode the temporal information within each of these sequences using our video feature extractor and then we scale each feature using their corresponding learned weight. In addition to these feature vectors, we construct another feature representation by taking the average of the output feature maps of Inception-V3 (top branch) and applying global average pooling (GAP) on the resulting tensor. Gf, Fb, Ub and Lb represent global feature, full body, upper body and lower body, respectively

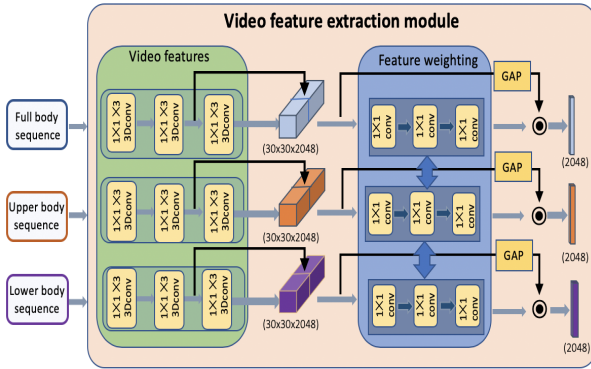


Figure 4: Video feature extraction module: Given three features attentioned to different body regions (upper, lower and full body), we aggregate the temporal information within each of these sequences using separate three $(1 \times 1 \times 3)$ 3D-convolution blocks, with spatial and temporal stride of 1 and 2, respectively. We then pass the concatenated features from the last and intermediate layers of video module to our weighting module to learn their respective weights. Finally, after applying global average pooling (GAP) on our final feature maps, we then scale them using their corresponding weights. We share parameters between all three feature weighting blocks.

(λ_1, φ_1) and (λ_2, φ_2) represent tuple of longitude and latitude of GPS_1 and GPS_2 , respectively.

For a camera, k , to be in a candidate set, \mathcal{S} , of target T_a^i , the following should hold: $H_a^i \equiv \mathbb{F}(C_{t^\tau}^{i^g}, C_{t^\tau}^{k^g})$. That is, for

a camera k to be selected as a candidate, its heading w.r.t the location of current camera of the target, $C_{t^\tau}^{i^g}$, is the same as target's heading H_a^i . Finally, the next camera for target a in camera i is estimated by selecting the closest camera at time t^τ among the candidate cameras, and is given by; $\arg \min_{C_{t^\tau}^j} \|G_a^i - C_{t^\tau}^{j^g}\|$, $\forall C_{t^\tau}^j \in \mathcal{S}$, where, G_a^i is GPS of target a of camera i at time t^τ and due to very close proximity of the cameras to the targets, we can approximate target's GPS by the camera i 's GPS at time t^τ , $C_{t^\tau}^{i^g}$.

Estimating time of arrival: Next, we estimate the time required to travel between camera i (current camera) and j (the next camera). Since our cameras topology is very dynamic (due to camera motion), we implicitly compute the time as a division of distance and speed. The speed of target a in camera i , \mathcal{V}_a^i , is estimated to be 1.3 m/s, which is the average walking speed of individual [40]. While the speed of camera j , $C_{t^\tau}^{j^v}$, can be inferred from the sensor meta-data. The distance between the next camera, j , and the target is computed between their GPS. Formally, the time required by target, T_a^i , to reach camera C^j , from camera i can be computed as follows:

$$\mathbb{E}(T_a^i, C^j) = \begin{cases} \frac{\|G_a^i - C_{t^\tau}^{j^g}\|}{|\mathcal{V}_a^i - C_{t^\tau}^{j^v}|}, & \text{if } H_a^i \equiv C_{t^\tau}^{j^h} \\ \frac{\|G_a^i - C_{t^\tau}^{j^g}\|}{|\mathcal{V}_a^i + C_{t^\tau}^{j^v}|}, & \text{Otherwise} \end{cases} \quad (1)$$

where H_a^i is the heading of target a at the time of exit, t^τ , from camera i and is inferred from its heading of camera i at time t^τ .

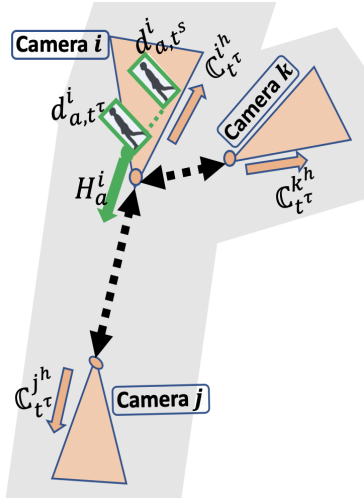


Figure 5: Camera Configuration Example: Lets assume the above topology represents the scene layout at time t^τ (at the time of exit of a target, shown in green boxes, from camera i . The orange triangles represent camera FOVs and their corresponding headings are indicated by the orange arrows. The black dotted lines shows the distance between camera i and the other two cameras. The green dotted line and arrow respectively represent a target’s tracklet and its heading. In this particular scenario, its evident that camera j should be selected as the *next camera*, since the target is heading towards it, even though camera k is closest camera to the target. And the estimated time is computed using the first case of eq. 1, as both camera j (*next camera*) and target have the same heading.

Note that in eq. 1, since both target and camera are moving, time computation depends on the direction of their motion. If both are moving in the same direction (i.e. same heading), first case in eq. 1, then we divide the distance by the difference of their speeds, otherwise, we estimate the time by dividing the distance with the sum of their speed.

Finally, we impose our time constraint on our appearance similarity. The final affinity between query target, T_a^i , and the rest of tracks, in camera \mathbb{C}^j , $T_l^j, \forall l = 1, \dots, |T^j|$, where $|T^j|$ is total number of tracks, is updated as follows:

$$M(T_a^i, T_l^j) = \begin{cases} \psi(\rho(T_a^i), \rho(T_l^j)), & \text{if } T_{l,t^s}^j \geq \mathbb{E}(T_a^i, \mathbb{C}^j) \\ 0, & \text{Otherwise} \end{cases} \quad (2)$$

where $\psi(\rho(T_a^i), \rho(T_l^j))$ is appearance similarity between two track features, T_{l,t^s}^j is an entrance time of track T_l^j . As can be inferred from eq. 2, during ReID, we only compare track T_a^i with tracks in camera j which appears after the estimated time of arrival. Thus, we can significantly reduce

our search space by pruning several wrong matching which violate our time constraint.

6. Experiments

6.1. Datasets

We present evaluation on proposed EgoReID dataset and widely used, *fixed cameras* dataset, MARS [59]. MARS consists of 6 cameras and 1261 different pedestrians. There are 625 identities for training and 636 identities for testing.

Evaluation settings: Training/Testing split of EgoReID dataset contains 567 identities for training and 309 identities for testing. For MARS dataset, we follow the same Training/Testing split setting as proposed by the authors of the dataset. To evaluate performance for each algorithm, we report the Cumulative Matching Characteristic (CMC) metric and mean average precision (mAP).

Training the Network: We first train the semantic segmentation module of our proposed model using Look Into Person (LIP) [19] dataset. We then freeze the semantic segmentation module for the rest of the training. We train our frame-level feature extraction module using the segmentation maps produced by semantic segmentation module. Since only 3 semantic regions are used in the model, we group the segmentation maps of different regions to create the segmentation maps for foreground, upper-body and lower-body. During the training of the frame-level feature extraction module, we use a training set consisting of 10 image-based ReID datasets. Next, we fine-tune the frame-level feature extraction module by image-based training using the images from the video datasets (MARS or EgoReID). In the last step of the training, we freeze frame-level feature extraction module and train video feature extraction module using video clips of 15 frames. As mentioned in Section 4, there are three consecutive 3D-convolution layers for each region. After concatenating feature maps from the last and intermediate layer, for each regions we produce a tensor of size $(30 \times 30 \times 2048)$. We then construct feature vectors from these tensors by applying GAP and then scale them using their corresponding weights. We then compute the loss for each region by performing multi-class classification. Final loss of the model is obtained by taking the average of three losses. More implementation details are provided in the supplementary material.

Ablation study We investigate the effect of each component of our model by conducting several experiments. In Table. 2, we show the results of each component in the proposed network. We evaluate the effects of each body regions and sensor meta data. As can be noted from Table. 2, lower body features perform worse on EgoReID, while they achieve reasonable result on MARS. This is mainly due to the fact that in EgoReID dataset lower body is frequently missing as the camera is very close to the target. We can

also observe from Table. 2 that, jointly using features from different body regions, leads to improvements in the performance than using only one body region.

We can also see that the proposed approach for using sensor information to prune several unreliable matches, significantly improves the ReID performance of our approach on EgoReID dataset. As shown in Table. 2, we are able to improve rank-1 and mAP by around 15% and 10%, respectively.

Methods	MARS		EgoReID	
	R-1	mAP	R-1	mAP
Upper body (Ub)	70.76	56.61	26.21	22.64
Lower body (Lb)	72.12	57.91	16.02	11.78
Full body (Fb)	77.22	63.71	28.41	25.68
Ub+Lb+Fb	80.01	67.96	35.16	30.51
Ub+Lb+Fb+Gf	83.18	72.91	38.84	34.62
Ub+Lb+Fb+Gf + Metadata	-	-	53.02	44.79

Table 2: Ablation study of our approach on MARS and EgoReID datasets. Gf are global features from frame-level feature extraction module.

We have also evaluated the contributions of our feature weighting module and multi-scale features. As observed from table 4, exploiting multi-scale features from intermediate layers improves our performance by 2% and 5% in rank-1 and mAP, respectively. Learning weights for each region features based on their discriminative abilities, improves our result by $\sim 2\%$ both in rank-1 and mAP.

To further show the effectiveness of the proposed model, we compare our results with [24], where we apply their method on frame by frame bases and then employ average pooling over temporal dimension to generate features from each region. As can be seen from Table. 3, our approach gives significantly better results in both rank-1 and mAP (i.e. 24% and 41% respectively). This shows the effectiveness of the proposed video feature extractor module.

Methods	R-1	R-5	mAP
SPReID [24] (Avg pooling)	58.23	72.07	31.21
Ours	83.18	93.28	72.91

Table 3: Comparison of SPReID [24] and the proposed approach on MARS dataset.

Comparison to state-of-the-art Methods: In Table. 5 and Table. 6, we compare our approach against the state-of-the-art methods on EgoReID and MARS, respectively. As can be observed from Table. 5, our approach significantly outperforms state-of-the-art approaches on EgoReID dataset. This shows the effectiveness of our human semantic region based local feature extraction approach on our dataset. This

Methods	R-1	R-5	mAP
Without both weights & multi-scale features	79.19	89.70	65.91
With multi-scale features	81.22	92.14	70.30
With multi-scale features and weights	83.18	93.28	72.91

Table 4: Ablation study of different components of our approach on MARS dataset.

is mainly due to different body parts of pedestrians being clearly visible in EgoReID. In Table. 6, we observe that our method was able to outperform current state-of-the-art approaches on MARS dataset in all rank 1,5 and mAP. This further demonstrates the robustness of our approach in handling different domains of video.

Methods	R-1	R-5	mAP
PSE+ECN [42]	15.17	25.79	8.58
MGCAM [44]	18.48	29.79	14.60
Ours	53.02	63.52	44.79

Table 5: Comparison to state-of-the-art on EgoReID dataset.

Methods	R-1	R-5	mAP
K-Res [65]	70.51	-	55.12
MSCAN [26]	71.77	-	56.05
SpaAtn [27]	82.30	-	65.8
PSE+ ECN [42]	76.70	-	71.8
MGCAM [44]	77.17	-	71.17
DuATN [43]	81.16	92.47	67.73
J. Zhang et al.[57]	71.20	85.70	71.8
Ours	83.18	93.28	72.91
Ours+RR	85.15	94.95	81.56

Table 6: Comparison to state-of-the-art on MARS dataset. RR is re-ranking using [42].

7. Conclusion

In this paper, we presented a new EgoReID dataset which is captured using 3 mobile cellphones with non-overlapping FOV. EgoReID dataset captures substantial variations in lighting, scene, background, human pose, etc. Compared to the existing video-based ReID datasets, EgoReID poses several realistic challenges to person ReID task. Unique feature of our dataset is that we also provide 12 sensor meta data for each video.

We also proposed a new method to solve EgoReID problem, where first frame level local features are extracted for each semantic region, then 3D convolutions are applied to

encode the temporal information in each sequence of semantic regions. Experiments conducted on MARS and EgoReID showed the effectiveness of our approach in different video domains. In addition, we have also successfully employed sensor meta data information to determine target's next camera and its estimated time of arrival, thus, we only search for a target in the predicted camera around the estimated time of arrival. This significantly improved our ReID performance by reducing our search space.

References

- [1] M. Aghaei, M. Dimiccoli, and P. Radeva. Multi-face tracking by extended bag-of-tracklets in egocentric photo-streams. *Computer Vision and Image Understanding*, 149:146–156, 2016.
- [2] A. Alahi, M. Bierlaire, and M. Kunt. Object detection and matching with mobile cameras collaborating with fixed cameras. In *Workshop on Multi-camera and Multi-modal Sensor Fusion Algorithms and Applications-M2SFA2 2008*, 2008.
- [3] A. Alahi, D. Marimon, M. Bierlaire, and M. Kunt. A master-slave approach for object detection and matching with fixed and mobile cameras. In *15th IEEE International Conference on Image Processing*, number CONF, 2008.
- [4] S. Ardeshir and A. Borji. Ego2top: Matching viewers in egocentric and top-view videos. In *European Conference on Computer Vision*, pages 253–268. Springer, 2016.
- [5] D. Baltieri, R. Vezzani, and R. Cucchiara. 3dps: 3d people dataset for surveillance and forensics. In *Proceedings of the 2011 joint ACM workshop on Human gesture and behavior understanding*, pages 59–64. ACM, 2011.
- [6] Y. Bengio, N. Boulanger-Lewandowski, and R. Pascanu. Advances in optimizing recurrent networks. In *2013 IEEE International Conference on Acoustics, Speech and Signal Processing*, pages 8624–8628. IEEE, 2013.
- [7] V. Bettadapura, I. Essa, and C. Pantofaru. Egocentric field-of-view localization using first-person point-of-view devices. In *Applications of Computer Vision (WACV), 2015 IEEE Winter Conference on*, pages 626–633. IEEE, 2015.
- [8] A. Borji, D. N. Sihite, and L. Itti. What/where to look next? modeling top-down visual attention in complex interactive environments. *IEEE Transactions on Systems, Man, and Cybernetics: Systems*, 44(5):523–538, 2014.
- [9] J. Carreira and A. Zisserman. Quo vadis, action recognition? a new model and the kinetics dataset. In *Computer Vision and Pattern Recognition (CVPR), 2017 IEEE Conference on*, pages 4724–4733. IEEE, 2017.
- [10] L.-C. Chen, G. Papandreou, F. Schroff, and H. Adam. Rethinking atrous convolution for semantic image segmentation. *arXiv preprint arXiv:1706.05587*, 2017.
- [11] W. Chen, X. Chen, J. Zhang, and K. Huang. Beyond triplet loss: a deep quadruplet network for person re-identification. In *The IEEE Conference on Computer Vision and Pattern Recognition (CVPR)*, volume 2, 2017.
- [12] A. Dehghan, S. Modiri Assari, and M. Shah. Gmmcp tracker: Globally optimal generalized maximum multi clique problem for multiple object tracking. In *Proceedings of the IEEE Conference on Computer Vision and Pattern Recognition*, pages 4091–4099, 2015.
- [13] A. Fathi, A. Farhadi, and J. M. Rehg. Understanding egocentric activities. In *Computer Vision (ICCV), 2011 IEEE International Conference on*, pages 407–414. IEEE, 2011.
- [14] A. Fathi, Y. Li, and J. M. Rehg. Learning to recognize daily actions using gaze. In *European Conference on Computer Vision*, pages 314–327. Springer, 2012.
- [15] A. Fathi, X. Ren, and J. M. Rehg. Learning to recognize objects in egocentric activities. In *Computer Vision and Pattern Recognition (CVPR), 2011 IEEE Conference On*, pages 3281–3288. IEEE, 2011.
- [16] P. F. Felzenszwalb, R. B. Girshick, D. McAllester, and D. Ramanan. Object detection with discriminatively trained part-based models. *IEEE transactions on pattern analysis and machine intelligence*, 32(9):1627–1645, 2009.
- [17] F. Fergnani, S. Alletto, G. Serra, J. De Mira, and R. Cucchiara. Body part based re-identification from an egocentric perspective. In *Proceedings of the IEEE Conference on Computer Vision and Pattern Recognition Workshops*, pages 1–6, 2016.
- [18] F. Ferland, F. Pomerleau, C. T. Le Dinh, and F. Michaud. Egocentric and exocentric teleoperation interface using real-time, 3d video projection. In *Proceedings of the 4th ACM/IEEE international conference on Human robot interaction*, pages 37–44. ACM, 2009.
- [19] K. Gong, X. Liang, D. Zhang, X. Shen, and L. Lin. Look into person: Self-supervised structure-sensitive learning and a new benchmark for human parsing. In *CVPR*, volume 2, page 6, 2017.
- [20] S. Gong, M. Cristani, S. Yan, and C. C. Loy. *Person re-identification*. Springer, 2014.
- [21] D. Gray, S. Brennan, and H. Tao. Evaluating appearance models for recognition, reacquisition, and tracking. In *Proc. IEEE International Workshop on Performance Evaluation for Tracking and Surveillance (PETS)*, volume 3, pages 1–7. Citeseer, 2007.
- [22] M. Hirzer, C. Beleznai, P. M. Roth, and H. Bischof. Person re-identification by descriptive and discriminative classification. In *Scandinavian conference on Image analysis*, pages 91–102. Springer, 2011.
- [23] H. Jiang and K. Grauman. Seeing invisible poses: Estimating 3d body pose from egocentric video. In *2017 IEEE Conference on Computer Vision and Pattern Recognition (CVPR)*, pages 3501–3509. IEEE, 2017.
- [24] M. M. Kalayeh, E. Basaran, M. Gökmen, M. E. Kamasak, and M. Shah. Human semantic parsing for person re-identification. In *Proceedings of the IEEE Conference on Computer Vision and Pattern Recognition*, pages 1062–1071, 2018.
- [25] Y. Kawanishi, Y. Wu, M. Mukunoki, and M. Minoh. Shinpuhkan2014: A multi-camera pedestrian dataset for tracking people across multiple cameras. In *20th Korea-Japan Joint Workshop on Frontiers of Computer Vision*, volume 5. Citeseer, 2014.
- [26] D. Li, X. Chen, Z. Zhang, and K. Huang. Learning deep context-aware features over body and latent parts for person

- re-identification. In *Proceedings of the IEEE Conference on Computer Vision and Pattern Recognition*, pages 384–393, 2017.
- [27] S. Li, S. Bak, P. Carr, and X. Wang. Diversity regularized spatiotemporal attention for video-based person re-identification. In *Proceedings of the IEEE Conference on Computer Vision and Pattern Recognition*, pages 369–378, 2018.
- [28] S. Li, T. Xiao, H. Li, B. Zhou, D. Yue, and X. Wang. Person search with natural language description. *arXiv preprint arXiv:1702.05729*, 2017.
- [29] W. Li and X. Wang. Locally aligned feature transforms across views. In *Proceedings of the IEEE Conference on Computer Vision and Pattern Recognition*, pages 3594–3601, 2013.
- [30] W. Li, R. Zhao, and X. Wang. Human reidentification with transferred metric learning. In *Asian Conference on Computer Vision*, pages 31–44. Springer, 2012.
- [31] W. Li, R. Zhao, T. Xiao, and X. Wang. Deepreid: Deep filter pairing neural network for person re-identification. In *Proceedings of the IEEE Conference on Computer Vision and Pattern Recognition*, pages 152–159, 2014.
- [32] Y. Li, A. Fathi, and J. M. Rehg. Learning to predict gaze in egocentric video. In *2013 IEEE International Conference on Computer Vision*, pages 3216–3223. IEEE, 2013.
- [33] J. Liu, A. Shahroudy, D. Xu, and G. Wang. Spatio-temporal lstm with trust gates for 3d human action recognition. In *European Conference on Computer Vision*, pages 816–833. Springer, 2016.
- [34] C. C. Loy, T. Xiang, and S. Gong. Multi-camera activity correlation analysis. 2009.
- [35] Z. Lu and K. Grauman. Story-driven summarization for egocentric video. In *2013 IEEE Conference on Computer Vision and Pattern Recognition*, pages 2714–2721. IEEE, 2013.
- [36] X. Ma, X. Zhu, S. Gong, X. Xie, J. Hu, K.-M. Lam, and Y. Zhong. Person re-identification by unsupervised video matching. *Pattern Recognition*, 65:197–210, 2017.
- [37] N. McLaughlin, J. Martinez del Rincon, and P. Miller. Recurrent convolutional network for video-based person re-identification. In *Proceedings of the IEEE conference on computer vision and pattern recognition*, pages 1325–1334, 2016.
- [38] J. Redmon and A. Farhadi. Yolo9000: better, faster, stronger. *arXiv preprint*, 2017.
- [39] E. Ristani, F. Solera, R. Zou, R. Cucchiara, and C. Tomasi. Performance measures and a data set for multi-target, multi-camera tracking. In *European Conference on Computer Vision*, pages 17–35. Springer, 2016.
- [40] T. Robin, G. Antonini, M. Bierlaire, and J. Cruz. Specification, estimation and validation of a pedestrian walking behavior model. *Transportation Research Part B: Methodological*, 43(1):36–56, 2009.
- [41] O. Russakovsky, J. Deng, H. Su, J. Krause, S. Satheesh, S. Ma, Z. Huang, A. Karpathy, A. Khosla, M. Bernstein, et al. Imagenet large scale visual recognition challenge. *International Journal of Computer Vision*, 115(3):211–252, 2015.
- [42] M. Saquib Sarfraz, A. Schumann, A. Eberle, and R. Stiefelhagen. A pose-sensitive embedding for person re-identification with expanded cross neighborhood re-ranking. In *Proceedings of the IEEE Conference on Computer Vision and Pattern Recognition*, pages 420–429, 2018.
- [43] J. Si, H. Zhang, C.-G. Li, J. Kuen, X. Kong, A. C. Kot, and G. Wang. Dual attention matching network for context-aware feature sequence based person re-identification. *arXiv preprint arXiv:1803.09937*, 2018.
- [44] C. Song, Y. Huang, W. Ouyang, and L. Wang. Mask-guided contrastive attention model for person re-identification. In *Proceedings of the IEEE Conference on Computer Vision and Pattern Recognition*, pages 1179–1188, 2018.
- [45] C. Szegedy, V. Vanhoucke, S. Ioffe, J. Shlens, and Z. Wojna. Rethinking the inception architecture for computer vision. In *Proceedings of the IEEE Conference on Computer Vision and Pattern Recognition*, pages 2818–2826, 2016.
- [46] Y. T. Tesfaye, E. Zemene, A. Prati, M. Pelillo, and M. Shah. Multi-target tracking in multiple non-overlapping cameras using fast-constrained dominant sets. *International Journal of Computer Vision*, May 2019.
- [47] R. R. Varior, M. Haloi, and G. Wang. Gated siamese convolutional neural network architecture for human re-identification. In *European Conference on Computer Vision*, pages 791–808. Springer, 2016.
- [48] F. Wang, W. Zuo, L. Lin, D. Zhang, and L. Zhang. Joint learning of single-image and cross-image representations for person re-identification. In *Proceedings of the IEEE Conference on Computer Vision and Pattern Recognition*, pages 1288–1296, 2016.
- [49] T. Wang, S. Gong, X. Zhu, and S. Wang. Person re-identification by discriminative selection in video ranking. *IEEE Trans. Pattern Anal. Mach. Intell.*, 38(12):2501–2514, 2016.
- [50] X. Wang. Intelligent multi-camera video surveillance: A review. *Pattern recognition letters*, 34(1):3–19, 2013.
- [51] T. Xiao, S. Li, B. Wang, L. Lin, and X. Wang. End-to-end deep learning for person search. *arXiv preprint arXiv:1604.01850*, 2, 2016.
- [52] S. Xu, Y. Cheng, K. Gu, Y. Yang, S. Chang, and P. Zhou. Jointly attentive spatial-temporal pooling networks for video-based person re-identification. *arXiv preprint arXiv:1708.02286*, 2017.
- [53] Y. Yao, M. Xu, Y. Wang, D. J. Crandall, and E. M. Atkins. Unsupervised traffic accident detection in first-person videos. *arXiv preprint arXiv:1903.00618*, 2019.
- [54] J. You, A. Wu, X. Li, and W.-S. Zheng. Top-push video-based person re-identification. In *Proceedings of the IEEE Conference on Computer Vision and Pattern Recognition*, pages 1345–1353, 2016.
- [55] F. Yu and V. Koltun. Multi-scale context aggregation by dilated convolutions. *arXiv preprint arXiv:1511.07122*, 2015.
- [56] S.-I. Yu, Y. Yang, and A. Hauptmann. Harry potter’s marauder’s map: Localizing and tracking multiple persons-of-interest by nonnegative discretization. In *2013 IEEE Conference on Computer Vision and Pattern Recognition*, pages 3714–3720. IEEE, 2013.

- [57] J. Zhang, N. Wang, and L. Zhang. Multi-shot pedestrian re-identification via sequential decision making. *arXiv preprint arXiv:1712.07257*, 2017.
- [58] H. Zhao, M. Tian, S. Sun, J. Shao, J. Yan, S. Yi, X. Wang, and X. Tang. Spindle net: Person re-identification with human body region guided feature decomposition and fusion. In *Proceedings of the IEEE Conference on Computer Vision and Pattern Recognition*, pages 1077–1085, 2017.
- [59] L. Zheng, Z. Bie, Y. Sun, J. Wang, C. Su, S. Wang, and Q. Tian. Mars: A video benchmark for large-scale person re-identification. In *European Conference on Computer Vision*, pages 868–884. Springer, 2016.
- [60] L. Zheng, Z. Bie, Y. Sun, J. Wang, C. Su, S. Wang, and Q. Tian. Mars: A video benchmark for large-scale person re-identification. In *European Conference on Computer Vision*, pages 868–884. Springer, 2016.
- [61] L. Zheng, L. Shen, L. Tian, S. Wang, J. Wang, and Q. Tian. Scalable person re-identification: A benchmark. In *Proceedings of the IEEE International Conference on Computer Vision*, pages 1116–1124, 2015.
- [62] L. Zheng, Y. Yang, and A. G. Hauptmann. Person re-identification: Past, present and future. *arXiv preprint arXiv:1610.02984*, 2016.
- [63] L. Zheng, H. Zhang, S. Sun, M. Chandraker, Y. Yang, Q. Tian, et al. Person re-identification in the wild. In *CVPR*, volume 1, page 2, 2017.
- [64] Z. Zheng, L. Zheng, and Y. Yang. Unlabeled samples generated by gan improve the person re-identification baseline in vitro. *arXiv preprint arXiv:1701.07717*, 3, 2017.
- [65] Z. Zhong, L. Zheng, D. Cao, and S. Li. Re-ranking person re-identification with k-reciprocal encoding. In *Computer Vision and Pattern Recognition (CVPR), 2017 IEEE Conference on*, pages 3652–3661. IEEE, 2017.
- [66] Z. Zhou, Y. Huang, W. Wang, L. Wang, and T. Tan. See the forest for the trees: Joint spatial and temporal recurrent neural networks for video-based person re-identification. In *Computer Vision and Pattern Recognition (CVPR), 2017 IEEE Conference on*, pages 6776–6785. IEEE, 2017.
- [67] X. Zhu, X.-Y. Jing, X. You, X. Zhang, and T. Zhang. Video-based person re-identification by simultaneously learning intra-video and inter-video distance metrics. *IEEE Transactions on Image Processing*, 27(11):5683–5695, 2018.

A. Appendices

We supplement our main submission in four aspects. **First**, we provide several details on our dataset. We have included plots, sample tracklets and videos to help better explain our EgoReID dataset. **Second**, to demonstrate the quality of our human semantic parsing model, we have included videos which show qualitative results of human semantic segmentation of sample tracklets. **Third**, to further elaborate the effectiveness of the proposed person ReID model, we have included qualitative results of some randomly selected queries. **Forth**, several implementation details are included.

B. EgoReID Dataset

In fig. 10 - 17, we show plots for several sensor meta data from camera 2, namely, heading, accelerometer, gravity, gyroscope, magnetic, orientation, rotation and speed.

Fig. 7 shows sample tracklets from each camera. Each row contain tracklets of the same person, while each column represent different camera. As can be noted from fig. 7, our dataset contains several illumination, pose and background changes both within and across cameras.

Fig. 8 and 9 provide more detailed statistics on our dataset. Camera 3 captures the most number of IDs and tracklets. Camera 2 captures the second most number of IDs but ranked third in total number of tracklets it contains.

Sample videos of detection and tracking results are included in the videos file. Moreover, we have included two video demonstrations for rotation, magnitude, orientation and gravity.

C. Qualitative Results

Person re-identification: In Fig. 18 – 19, given different example queries from EgoReID dataset, top 10 retrieved tracklets from the gallery are shown for different methods. In all examples, the first row shows the results obtained using Inception-v3, where we extract frame level global features and perform average pooling for each tracklet. The second row shows results, when we apply SPReID [24] on every frame in a tracklet and apply average pooling along the temporal dimension. While the third and fourth rows show results of our method before and after employing sensor meta data information. Correctly matched tracklets are shown with green boxes while the incorrect ones are show in red. To avoid clutter, we only show three frames per tracklet even though the length of tracklets in our dataset ranges between 16 and 31.

Semantic Segmentation: To show the quality of our human semantic parsing model, we have provided videos which demonstrate the segmentation quality on randomly sampled tracklets from MARS [60] and EgoReID datasets. In our videos, for better visualization, the original image, full body segmentation, and upper and lower body segmentations are shown side by side.

D. Implementation Details

Fig.6 details the architecture of our video feature extraction module. Fig.6(a) shows one block of our video feature extraction module. All 3 block in this module have the same architecture. To exploit multi-scale information, after applying average pooling along the temporal dimension, we concatenate feature maps from intermediate layer with the output of the last layer. Similarly, Fig.6(b) depicts the details of the proposed feature weighting module. We share parameters between our feature weighting modules. After

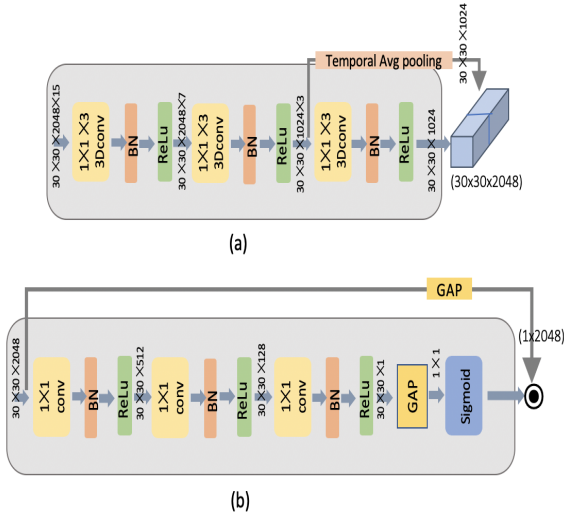


Figure 6: Detailed architecture used in our video feature extraction module. (a) shows one block of video feature extractor, the rest of the blocks have the same architecture. (b) shows details of a block from feature weighting module. We share weights between all blocks in feature weighting module.

applying global average pooling (GAP) on the output feature maps from video feature extraction module, we then use their corresponding weights to scale them.

Parameters: We train the Frame-level feature extraction module for 200K iterations using the training set consists of 10 image-based ReID datasets (Market-1501 [61], CUHK01 [30], CUHK02 [29], CUHK03 [31], DukeMTMC-reID [64], 3DPeS [5], PRID [22], PSDB [51], Shinhuhkan [25] and VIPeR [21]), then fine-tune it on the video datasets for 20K iterations. The initial learning rates for these two processes are 0.01 and 0.001, respectively, and we decay them 10 times with the rate of 0.9 by utilizing the exponential shift. Similarly, we use 0.001 as the learning rate while training the video feature extraction module and decay it 10 times. While training the Frame-level feature extraction module, the batch size, momentum and weight decay are 15, 0.9 and 0.0005 for the respective values. To train the video feature extraction module, we set the batch size to 6 and the length of the clips to 15. The input images with the size of 512×170 are used to train both the frame-level feature extraction module and the video feature extraction module.

We follow the same settings mentioned in [24] to train the semantic segmentation module. We set the initial learning rates to 0.01, 0.1 and 0.1 for the Inception-V3 backbone, atrous spatial pyramid pooling and the 1×1 convolution layer (classification layer), respectively, and decay them 10

times. The minibatch size is set to 8 and the input images with the size of 512×512 are used. The other settings are similar to the mentioned above. We perform the training of the re-identification and the segmentation models using Nesterov Accelerated Gradient [6] and used the pre-trained InceptionV3 models on ImageNet [41].

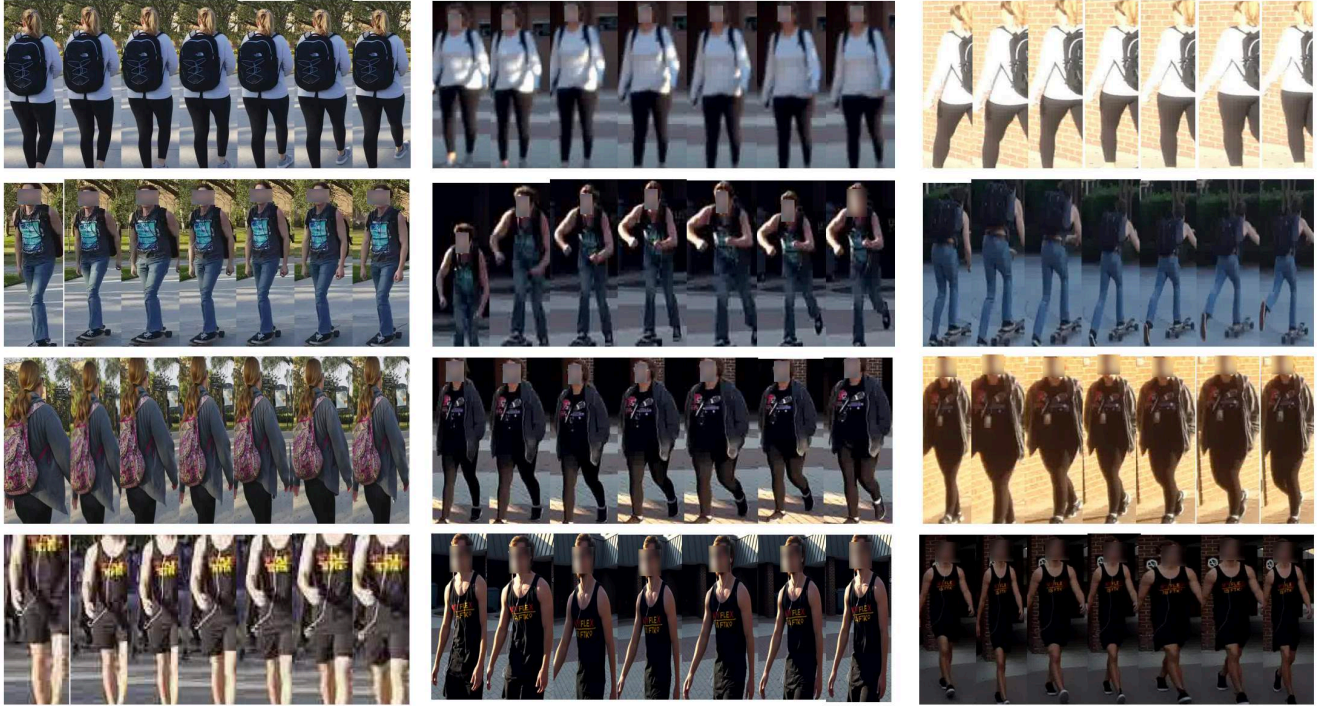


Figure 7: Sample tracklets from EgoReID. Each row corresponds to different identities, while each panel (from left to right) represents tracklets from cameras 1, 2 and 3. As can be noted, in addition to changes in background, pose and illumination of the same tracklet across camera (each row), due to camera motion, different tracklets from the same camera (each panel) are also captured with different background, illumination and poses. This makes our dataset challenging but more close to the reality. In the above figure, for the sake of better visualization, we resize pedestrian detection boxes to the same size, but in our dataset they are of different sizes.

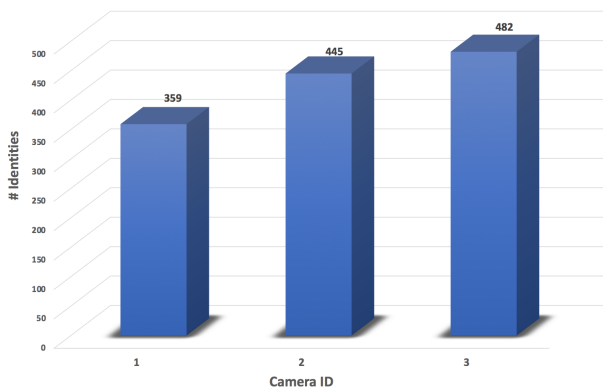


Figure 8: The number of IDs captured by each camera.

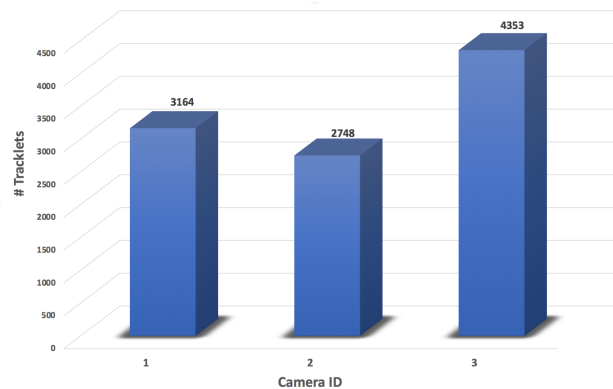


Figure 9: The number of tracklets per each camera.

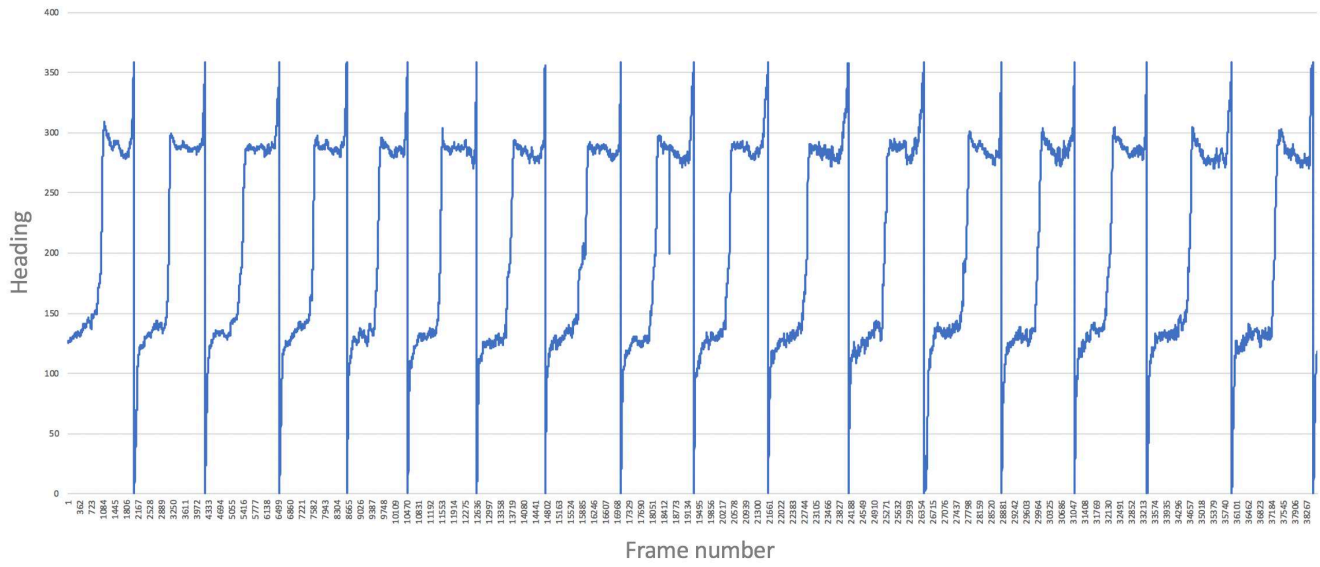


Figure 10: Heading plot.

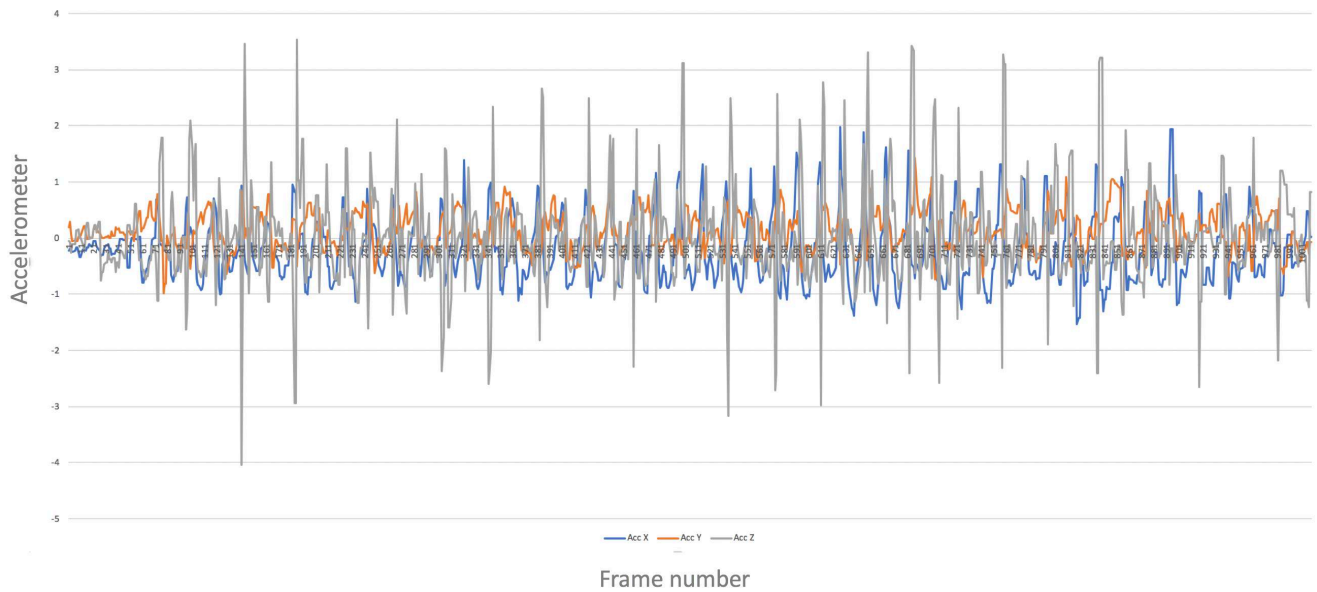


Figure 11: Accelerometer (x,y,z) plot.

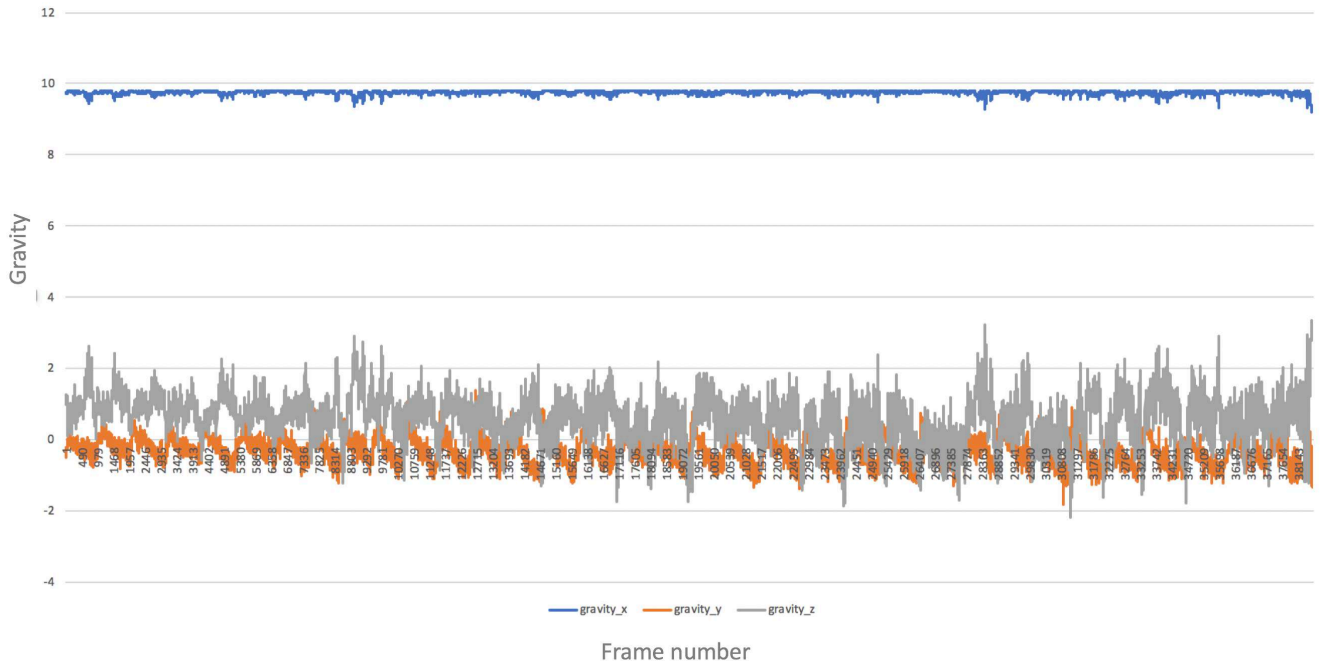


Figure 12: Gravity (x,y,z) Plot.

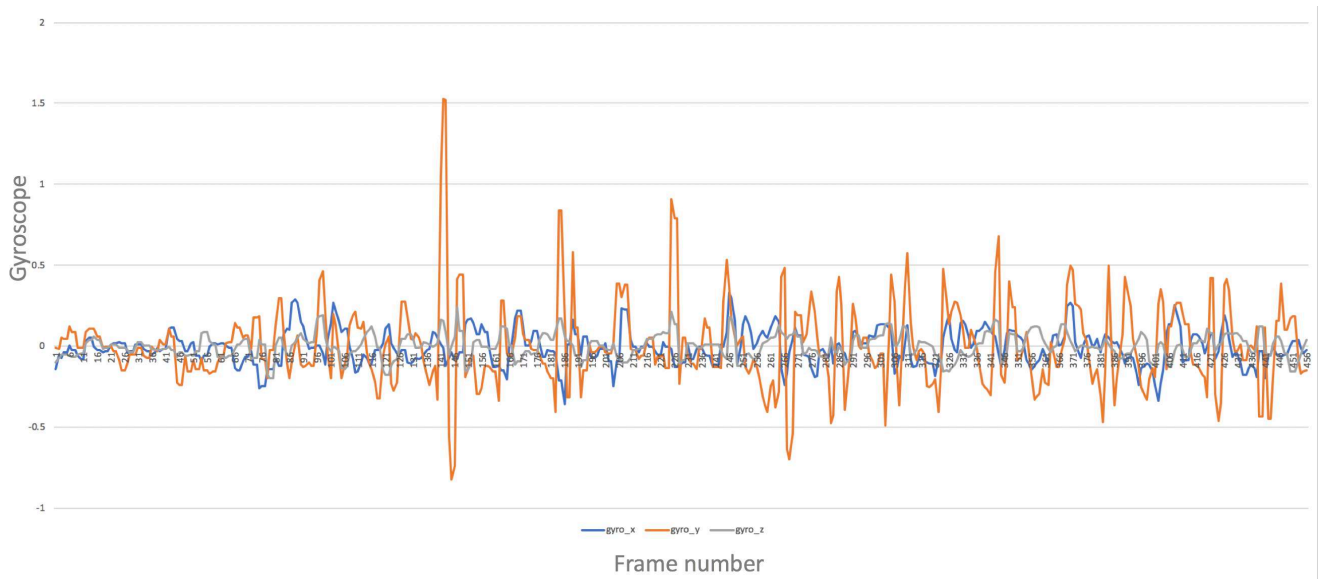


Figure 13: Gyroscope (x,y,z) plot.

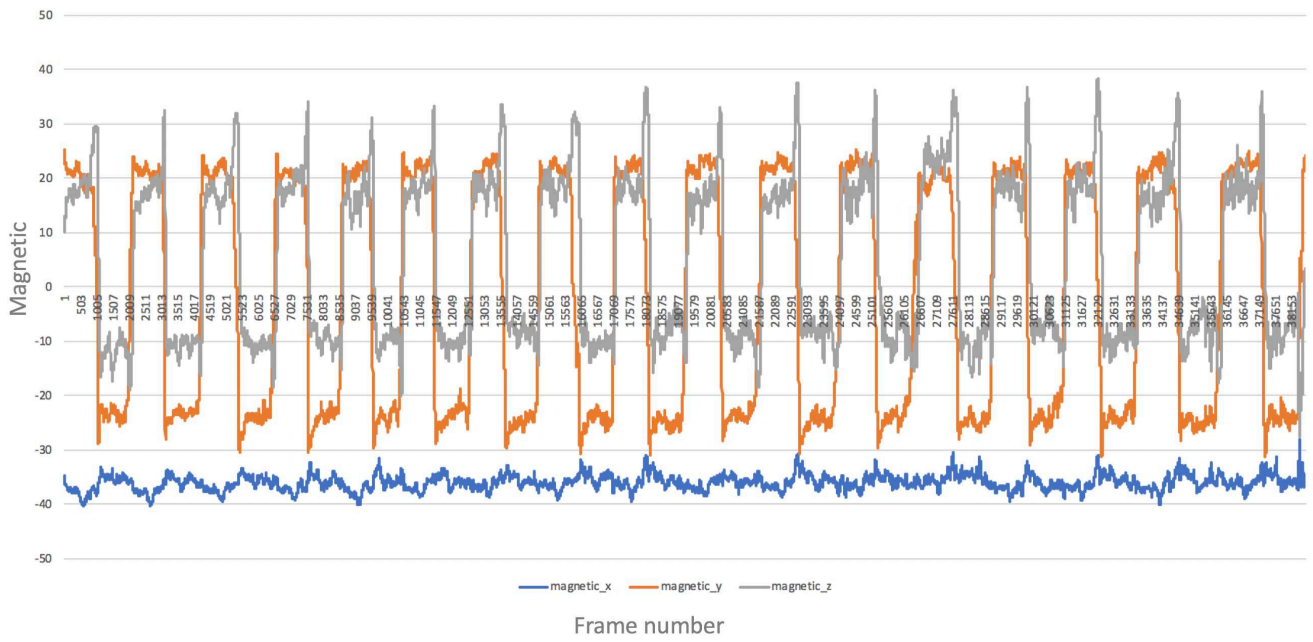


Figure 14: Magnetic (x,y,z) Plot.

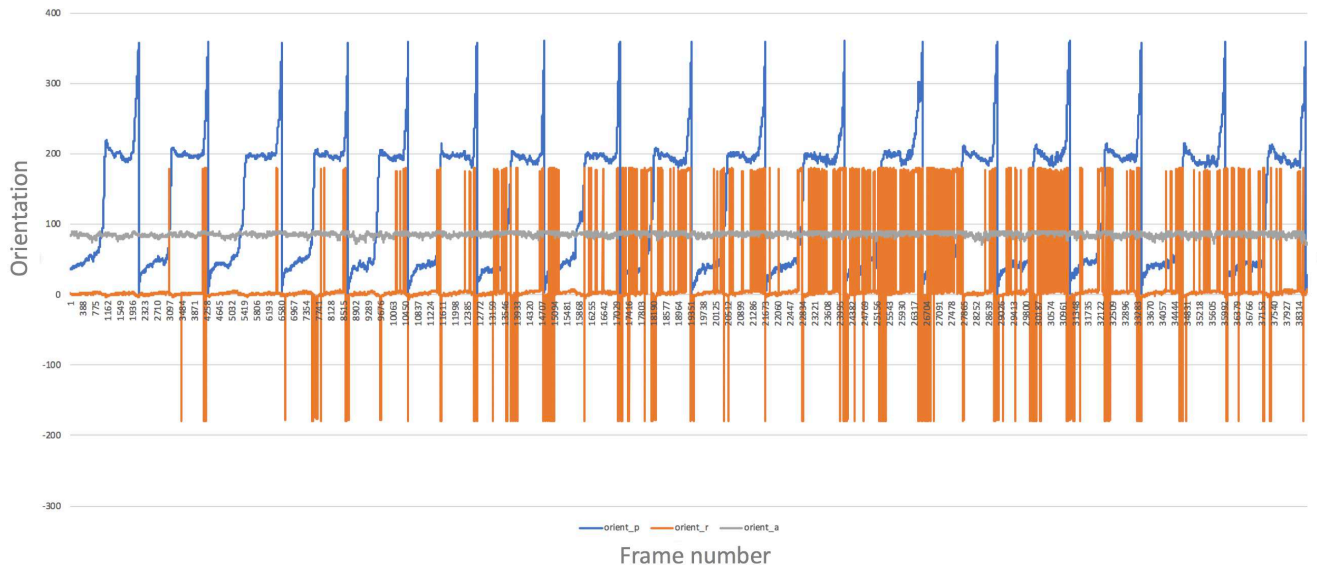


Figure 15: Orientation (x,y,z) plot.

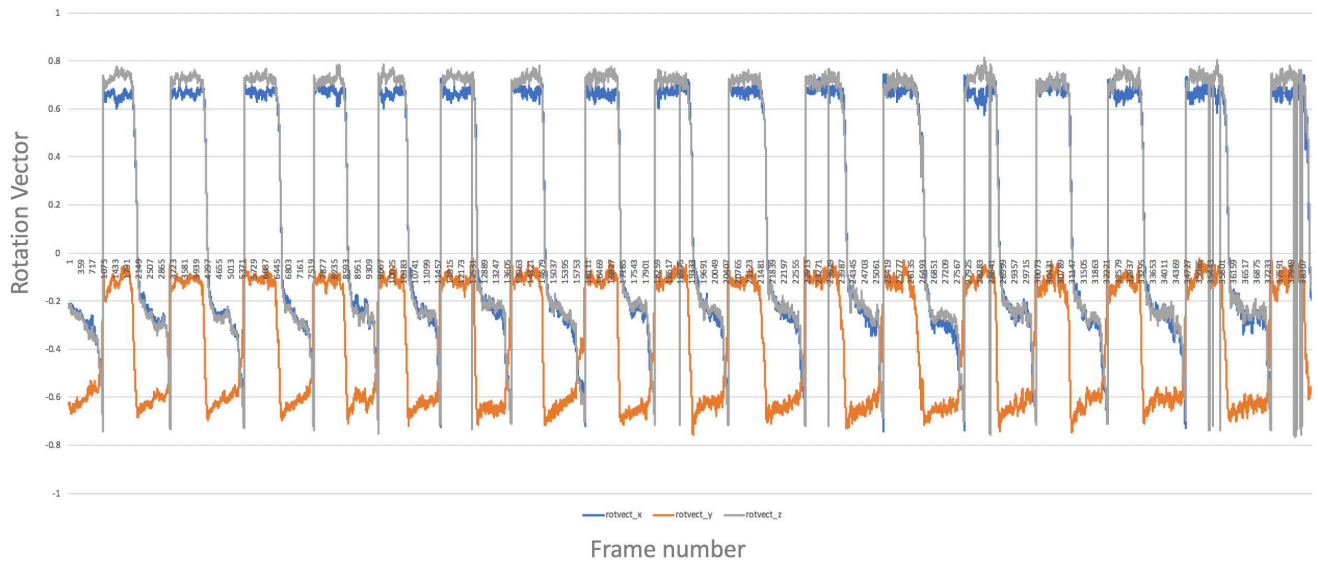


Figure 16: Rotation_Vector (x,y,z) plot.

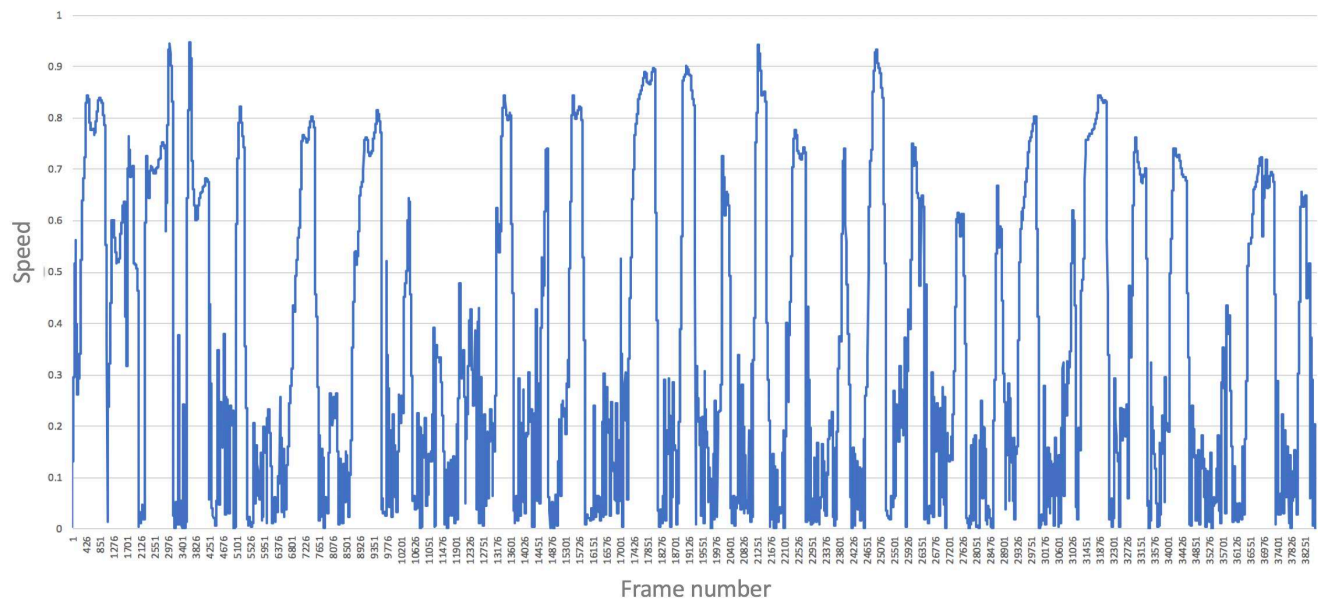


Figure 17: Speed plot.



Figure 18: Inception-v3 and our approach without meta data are able to find the correct match among top-4. However, after refining our results using sensor meta data, we are able to get the correct match at rank-1.

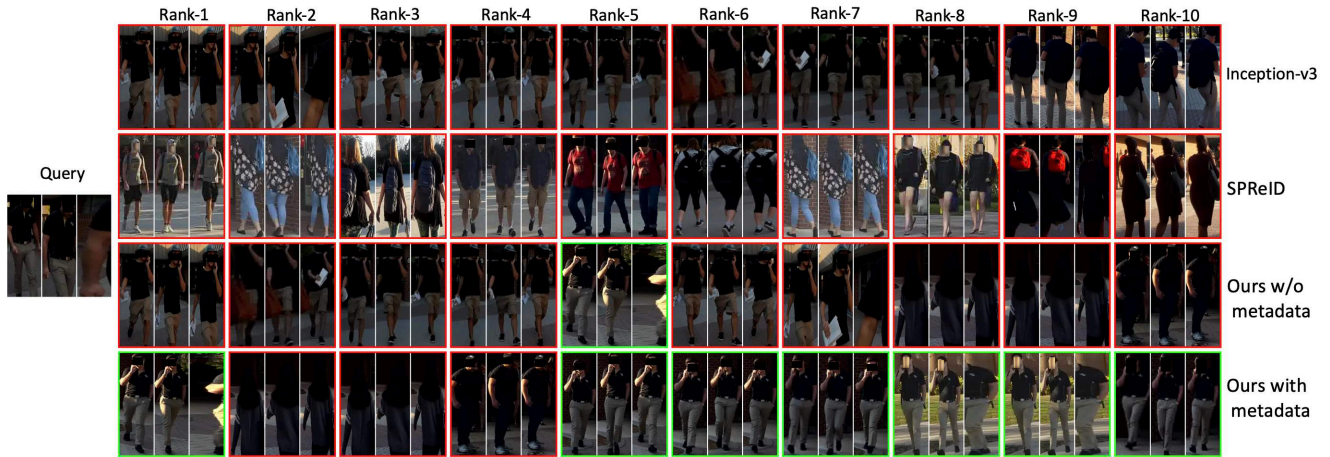


Figure 19: As it is evident that due to heavy occlusion of query tracklet, most approaches fail to find the correct match among their top-10 results. Our method without using meta data finds the correct match at rank-5, while after applying meta data information the correct match is found at rank-1.